Undersampled Projection Reconstruction Applied to MR Angiography

Dana C. Peters,[1]* Frank R. Korosec,[2,3] Thomas M. Grist,[3] Walter F. Block,[2] James E. Holden,[2,3] Karl K. Vigen,[2] and Charles A. Mistretta[2,3]

Undersampled projection reconstruction (PR) is investigated as an alternative method for MRA (MR angiography). In conventional 3D Fourier transform (FT) MRA, resolution in the phase-encoding direction is proportional to acquisition time. Since the PR resolution in all directions is determined by the readout resolution, independent of the number of projections (N_p), high resolution can be generated rapidly. However, artifacts increase for reduced N_p. In X-ray CT, undersampling artifacts from bright objects like bone can dominate other tissue. In MRA, where bright, contrast-filled vessels dominate, artifacts are often acceptable and the greater resolution per unit time provided by undersampled PR can be realized. The resolution increase is limited by SNR reduction associated with reduced voxel size. The hybrid 3D sequence acquires fractional echo projections in the k_x–k_y plane and phase encodings in k_z. PR resolution and artifact characteristics are demonstrated in a phantom and in contrast-enhanced volunteer studies. **Magn Reson Med 43:91–101, 2000.** © 2000 Wiley-Liss, Inc.

Key words: rapid imaging; projection reconstruction; contrast-enhanced; sparse sampling

Projection reconstruction (PR) imaging was one of the earliest imaging techniques in MRI (1) and lately is the subject of renewed interest. Investigators have shown the utility of PR in reduction of motion artifacts (2). Its characteristic of sampling some high and low spatial frequencies in each acquired projection has been exploited for dynamic imaging of moving objects by several investigators. Rasche et al. (3) used undersampled PR to image joint motion using a sliding window reconstruction. Another recent application is undersampled PR for catheter-tip tracking (4,5). PR also permits FID imaging of short T_2^* anatomy (6,7) because it is conducive to short echo times (8).

In PR, low spatial frequency data are accumulated with a higher density than high spatial frequency data. This results in a factor of $\pi/2$ increase in the data collection time required for artifact–free reconstruction for a field of view (FOV) and resolution comparable to spin-warp (Fourier transform, FT) imaging.

FT methods (9) generally provide images of higher quality than PR because of their immunity to off-resonance effects and k-space trajectory error (10). Chemical shift and B_0 inhomogeneity cause blurring in PR but not in FT methods. Short data readout times for each projection (large bandwidth-per-pixel), possible today because of stronger gradient strengths, reduce the blurring in PR, while reducing signal-to-noise ratio (SNR). PR is not widely used for clinical MR imaging due to these limitations.

Some investigators have recently applied reduced FOV techniques (11,12) to the PR acquisition (13,14) to improve resolution over a small FOV. In those studies, the goal was to acquire high-resolution images rapidly in a small dynamically changing FOV within a larger static FOV. We have recently reported (15) potential resolution advantages throughout the FOV using undersampled PR for MR angiography (MRA). Our initial work suggests that the spatial resolution that can be acquired in a given acquisition time using undersampled PR is uniform throughout the FOV and is similar to that normally associated with reduced FOV techniques. This increased resolution is accompanied by artifacts that appear to be tolerable.

For contrast-enhanced PR, weighting of k-space due to contrast agent passage differs from FT methods because the radial k-space path of PR acquires some high and low spatial frequencies with each TR. For FT imaging, the artifacts caused by modulation of k-space signal due to contrast agent passage can be serious and have been widely investigated (16). They have not been examined previously for PR. In this article we show the results of applying undersampled PR to contrast-enhanced MRA using two schemes for acquiring data during contrast agent infusion.

THEORY AND SIMULATIONS

It is well known in FT imaging that the reconstructed FOV is inversely proportional to the k-space sampling interval. Because of this relationship, higher resolution per unit time can be obtained when the FOV is decreased. For a fixed pixel size, larger k-space step size permits faster traversal of the required k-space. However, if signal is detected from an object outside of this FOV, aliasing results, wherein the object outside of the FOV is replicated within the FOV. Thus, reduced FOV FT imaging is only possible when aliasing is absent or overlays anatomy of no clinical value.

The case of undersampled PR is illustrated in Fig. 1. Suppose that the radial k-space sampling interval Δk_r
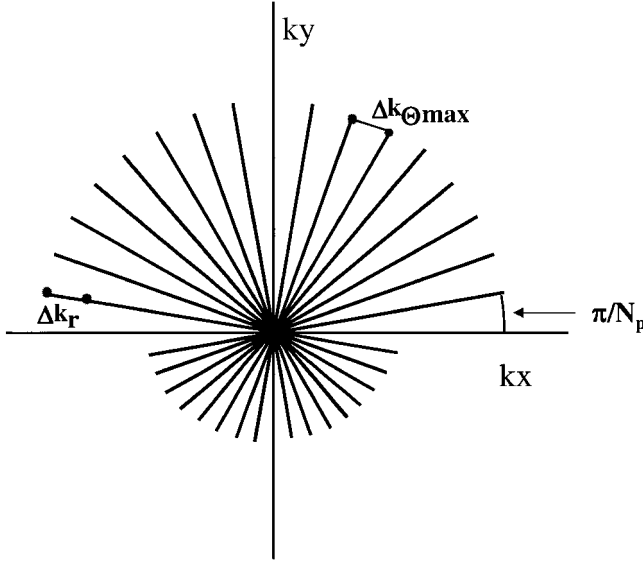
FIG. 1. The k-space path for PR. Fractional echoes are acquired through 180°. Δk_r is the radial spacing of samples and $\Delta k_{\Theta max}$ is the largest angular spacing between samples. In undersampled PR $\Delta k_{\Theta max} > \Delta k_r$. The angular step size, π/N_p, is shown. The radial k-space path length is given by $\Delta k_r \cdot N_r/2$ where $N_r/2$ is the number of samples along each radius.

would be sufficient to reconstruct N_r pixels along a distance D:

$$D = 1/\Delta k_r \qquad [1]$$

When the number of projections N_p is just sufficient to ensure that the maximum distance between k-space samples, Δk_Θ, is no larger than Δk_r, an FOV of diameter D is properly reconstructed. However, when N_p is reduced, the k-space steps Δk_Θ (see Fig. 1) in the azimuthal direction exceed Δk_r and alias-free reconstruction is only possible within an FOV of reduced linear dimension, d. This is given by the inverse of the arc length Δk_Θ:

$$d = 1/\Delta k_{\Theta max} = [(\pi/N_p) \cdot (\Delta k_r N_r/2)]^{-1} = 2N_p/(\pi \Delta k_r N_r) \quad [2]$$

Therefore, the reduced FOV, rFOV, supported by N_p projections is related to the full FOV supported by the radial sampling as follows:

$$rFOV/FOV = d/D = (N_p/N_r) \cdot 2/\pi \qquad [3]$$

The condition that rFOV = FOV is that $N_p = N_r \cdot \pi/2$. For this reason, fully sampled PR requires scan times $\pi/2$ times longer than conventional FT for the same matrix. Acquiring fewer projections will result in artifacts due to inadequate sampling and aliasing of high spatial frequencies.

In the image domain, an undersampled PR image of a point object (the point spread function) anywhere in the image has a well-reconstructed region rFOV, centered at the object. Even when the rFOV is significantly smaller than the overall image FOV, the spatial resolution is determined by the radial readout resolution and is roughly independent of N_p. Artifacts due to the point object are negligible within the rFOV. Radial streak artifacts, emanating from the object, become apparent outside the rFOV.

These artifacts contribute to the signal at distant points within the image. Similarly, the signal at each point within the image contains artifacts from all points separated from it by rFOV or more. This is illustrated in Fig. 2, which shows simulation results for the case of two objects reconstructed on a 256 × 256 matrix using only 64 projections. The input image is shown in Fig. 2a. As shown in Fig. 2b,c, when either object is separately reconstructed with undersampled PR, the object is surrounded by an alias-free region (rFOV) with a diameter one-sixth that of the full FOV. However, the object contributes artifacts to the rest of the FOV. In Fig. 2d, both objects are simultaneously reconstructed. Since the reconstruction process is linear, the artifacts produced by each object appear in the region of the other object. Nowhere is the reconstruction alias-free.

Provided that these artifacts can be tolerated, undersampled PR rapidly produces high-resolution images throughout the FOV. In theory, as the number of projections is reduced the spatial resolution, which is determined by the radial readout resolution, remains unchanged. In practice, the reduction of projections causes reduced SNR and greater artifact. There is a limit to the reduction of projections, beyond which higher resolution cannot be supported by the SNR or seen through the artifact.

MATERIALS AND METHODS

Data Collection and Reconstruction

A fast 3D gradient echo sequence was modified to collect projections in the k_x–k_y plane. Fourier-encodings in the k_z direction are used for 3D imaging. The pulse sequence is shown in Fig. 3. The excitation RF pulses employed are either a slab-selective asymmetrically truncated sinc RF
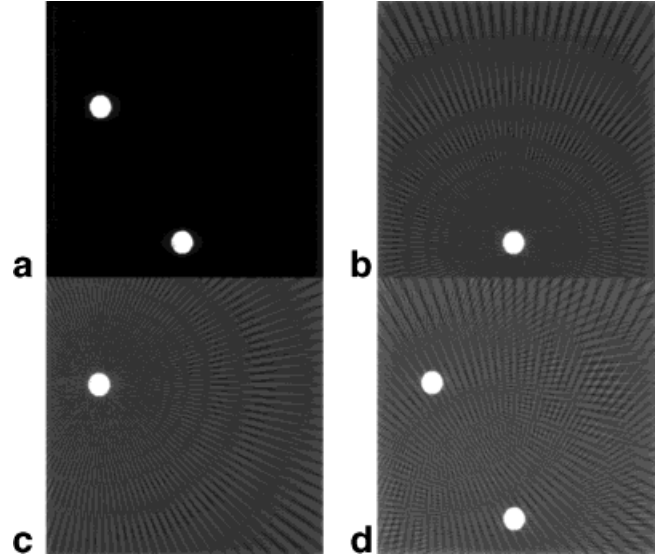

FIG. 2. **a:** Two input objects. These are shown in (**b**) and (**c**) after being separately reconstructed on a 256 × 256 grid using only 64 projections. Within reduced FOVs centered at each object, each object is properly reconstructed. However, each object contributes artifacts outside of its local reduced FOV. The radial streaks are the PR undersampling artifacts. **d:** A 64-projection reconstruction with both objects present. Each object is still properly reconstructed but creates artifacts everywhere except in its own reduced FOV. The window of these simulation images was set to display the artifacts.
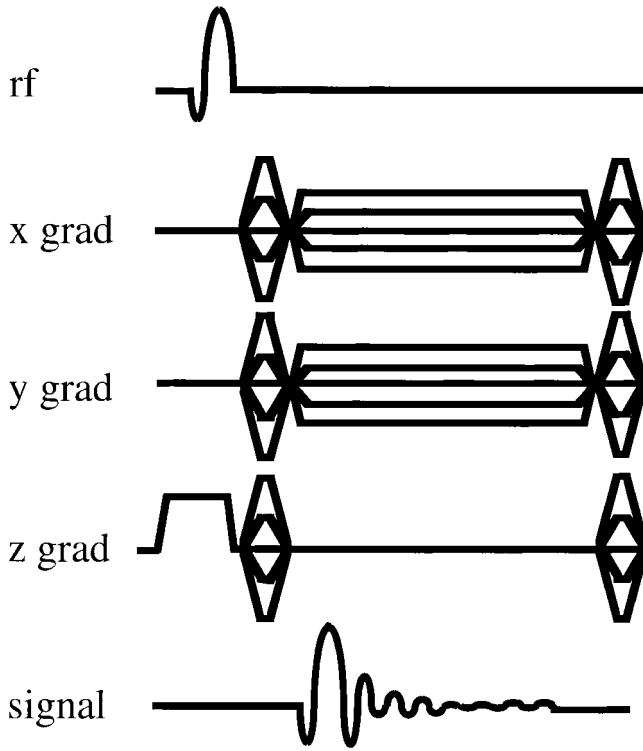
FIG. 3. The 3D PR sequence uses slab-selection and partition-encoding in the k_z direction. The projections are acquired as fractional echoes at a series of angles in the k_x–k_y plane. Optional x and y phase rewinders remove phase accumulation.

pulse of 0.5 ms duration, or a 1.28 ms minimum phase pulse. The z gradient is used for slab selection and Fourier-encoding in the k_z-direction. The x and y gradients shown are for prephasing and fractional-echo readout. Also shown are optional gradients played at the end of the sequence to rephase the phase accumulation from varying the readout gradients for each projection angle. High receiver bandwidths (± 64 kHz) are commonly used to reduce blurring due to off-resonance spins. Since fat is a bright off-resonance signal, blurring from this source is reduced by fat suppression. Fat suppression also reduces undersampling artifacts from fat. Fat suppression was employed using a chemically selective presaturation pulse followed by gradient dephasers, played separately (TR = 10 ms) every few TRs. The frequency of the fat suppression pulse depends on the acquisition order, as discussed below. TRs are reduced to their lowest values (typically 7–8 ms) possible using a Signa Horizon 1.5 T scanner equipped with slew rates of 120 mT/m /s and 22 mT/m maximum gradient strength. The projections were acquired as fractional echoes at angles through 180°, as shown in Fig. 1. Flip angles were set near the Ernst angle (typically 30–40°) for T_1-shortened blood. Image quality improved if not only the RF pulses but also the varying gradient amplitudes were cycled in disabled acquisitions at the start of the scan.

The reconstructions were performed off-line on a Silicon Graphics workstation. A Ram-Lak filter was used as suggested by Joseph (17) with the option of a Shepp-Logan filter. We acquired k-space in fractional echoes (60% asymmetric echoes) to reduce echo time compared to full echoes or to decrease scan time compared to k-space paths that begin at the origin. We first experimented with *magnitude* back projection, performing homodyne on a projection-by-projection basis and removing the phase from each projection before backprojecting. This provides reasonable images in phantoms and humans using phaseless image-space projections. However, we have found that *complex* back projection provides more accurate reconstruction. In complex backprojection, the real and imaginary channels are backprojected separately. This reconstruction requires that the center of the acquired k-space line is known exactly, and the k-space data is shifted accordingly before reconstruction. Furthermore, if the center of the FOV is shifted away from physical gradient center, the receiver frequency and the receiver phase must be carefully set for each projection angle.

The alternative method for reconstructing PR data, regridding followed by FT, produced images similar to complex backprojection for our data, with tradeoffs between SNR and resolution as described by Lauzon and Rutt (18). The aliasing pattern due to undersampling was not different between the two methods.

After complex backprojection or regridding, homodyne can be performed by modification of 2D FT homodyne (19,20). The high spatial frequencies are recovered and the SNR is reduced by about 30% relative to full echo acquisition, in accordance with expected SNR loss. Homodyne, compared to the option of zero-filling, boosts the amplitude of high spatial frequencies by two, but decreases the SNR (21). The slight spatial warp due to nonlinear gradients can be removed (10).

3D Contrast-Enhanced PR Acquisition Strategies

For contrast-enhanced imaging, we present two approaches. As illustrated in Fig. 4, both approaches acquire projections in the k_x–k_y plane and partition-encodings in the k_z-direction. The two approaches differ only in the order in which k-space data are collected.

In the first method, ZIPR (kZ-encodings Inside PRojections) (see Fig. 4), all of the partition-encodings are acquired for each projection prior to incrementing the projection angle. The acquisition proceeds for a time longer than that required to reconstruct a single time frame. Multiple time frames can be formed using a sliding temporal window to choose complete sets of projections for reconstruction (3). Because all k_z information is acquired for each projection in 80–200 msec (= Nz • TR), there is very little contrast-induced modulation in the k_z direction. Projection data can be modulated by the contrast curve, resulting in angular variations in signal in the x–y plane. Using a centric k_z-encoding order, fat suppression was achieved by playing the fat suppression pulse once each slice loop, before acquisition of the central k_z-encoding. This increases scan time by about 10 %.

ZIPR data contain an estimate of the average contrast-enhancement in the FOV throughout the scan. If during contrast agent infusion the signals from the entire FOV are monitored repeatedly, a contrast curve can be obtained. Following the Fourier transform in the radial and k_z direction, each projection can be used to obtain the sum of
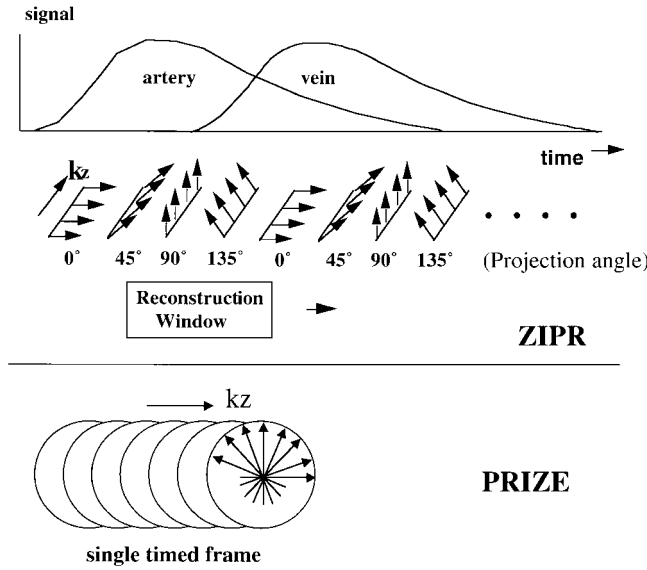
FIG. 4. The ZIPR and PRIZE acquisitions are shown in relation to hypothetical arterial and venous contrast curves. For the ZIPR acquisition, all partition-encodings are completed before incrementing the projection angle. The projection angle is rotated through several revolutions to provide several complete angular datasets. A sliding reconstruction window is used to provide flexibility in choosing the position of reconstructed frames relative to the contrast curves. In PRIZE, projections at all angles are acquired prior to incrementing the partition-encoding. PRIZE provides one timed or triggered frame using k_z-centric contrast weighting.

signals in each slice. Except for variations produced by anatomy not present in all projections, this sum is a constant for all projection angles, in the absence of contrast-enhancement, i.e.:

$$\int P(r, \theta) \cdot dr = \text{constant} \qquad \text{for all } \theta$$

Therefore, the ZIPR acquisition provides an estimate of the contrast curve with a temporal resolution of $N_z \cdot TR$ (the time between successive projections), typically 150 msec. This provides useful information about the arrival time of the contrast agent, and indicates which reconstructed time frames might be optimal.

In the second method, PRIZE (PRojections Inside kZ-Encodings) (see Fig. 4), all of the projections are collected for each sequential partition-encoding. Because the entire set of projections is collected for each partition-encoding, there is little contrast modulation in the k_x–k_y plane; all substantial modulation occurs in the k_z-direction. Therefore, contrast-induced artifacts, if present, will appear in the slice direction. Fat suppression was not employed in the PRIZE acquisitions, but it could in principle be performed every few TRs.

It is essential to time the PRIZE acquisitions so that the center of k_z-space is acquired during peak contrast, as in conventional FT. This reduces venous contamination and contrast agent-induced artifacts (16). In PRIZE, centric k_z encoding may be used. However, since there is no phase encoding in the k_x–k_y plane, elliptical-centric (k_z–k_y) encoding is not an option (22).

Phantom Studies

To demonstrate and quantitatively understand the resolution of undersampled PR, we acquired images of a resolution phantom on the MRI scanner with PR and FT acquisitions. The resolution phantom has dot patterns with spacings of 0.5 mm (smallest pattern), 0.75 mm, 1.0 mm and 2.0 mm (largest pattern). The images were all acquired on the MR scanner with 512 readout resolution and identical scan parameters. PR images with 128 projection angles and FT images with 512 and 128 phase encodings were obtained. The resolution phantom was also imaged with a 512 FT acquisition with FOV increased by 1.3, which we call a "400 × 400" FT acquisition, to place a lower limit on the resolution of undersampled PR.

Our hypothesis is that the PR image with 512 x 128 acquisition will have resolution equivalent to the 512 x 512 FT images. Filtering, homodyne detection, and backprojection (18) all influence resolution. For purposes of quantitation, these images were reconstructed without fermi-filtering; the PR data were reconstructed with regridding and a Ram-Lak filter.

Human Studies

Informed consent was obtained for all volunteers. The total contrast agent dose in all examinations was limited to 0.3 mmol/kg of gadolinium contrast agent. In some cases this was shared between multiple scans. The injection rates were between 0.5 and 3 ml/sec. A torso phased-array coil was used for the abdominal and pelvic examinations. A single-element neck coil was used for the carotid artery examination.

RESULTS

Phantom Studies

To obtain an understanding of the resolution differences between undersampled PR and fully sampled FT, a resolution phantom was imaged using PR and FT acquisitions. The Fourier resolution was 0.33 × 1.33 mm for the 512 × 128 FT, and 0.33 × 0.33 mm for the 512 × 512 FT. Magnified views of the resolution pattern displaying the resolution in the Fourier phase encoding (R-L) direction are shown in Fig. 5. Visually, the PR acquisition (Fig. 5b) has higher resolution than the FT acquisition, with 512 readout resolution and 128 phase encodings (Fig. 5a) and resolution similar to the 512 × 512 FT image (Fig. 5c), even though it was acquired in one-fourth the scan time. All of the images were acquired on the MRI scanner.

To quantify the resolution improvement, Fig. 6 compares the ability of four acquisitions to record the oscillations of dot patterns shown in Fig. 5. The difference between the mean signals within the patterns and the mean intermediate signals divided by the mean signals is plotted for each pattern, from largest to smallest, for the different acquisition methods. Signal measurements were made using cross-sections through the dot patterns. Figure 6 shows that the 512 × 128 PR image has resolution very similar to the 512 × 512 FT image. The resolution of the 512 × 128 PR image is far better than that of the 512 × 128 FT image in the phase encoding direction. The 512 × 128 PR has
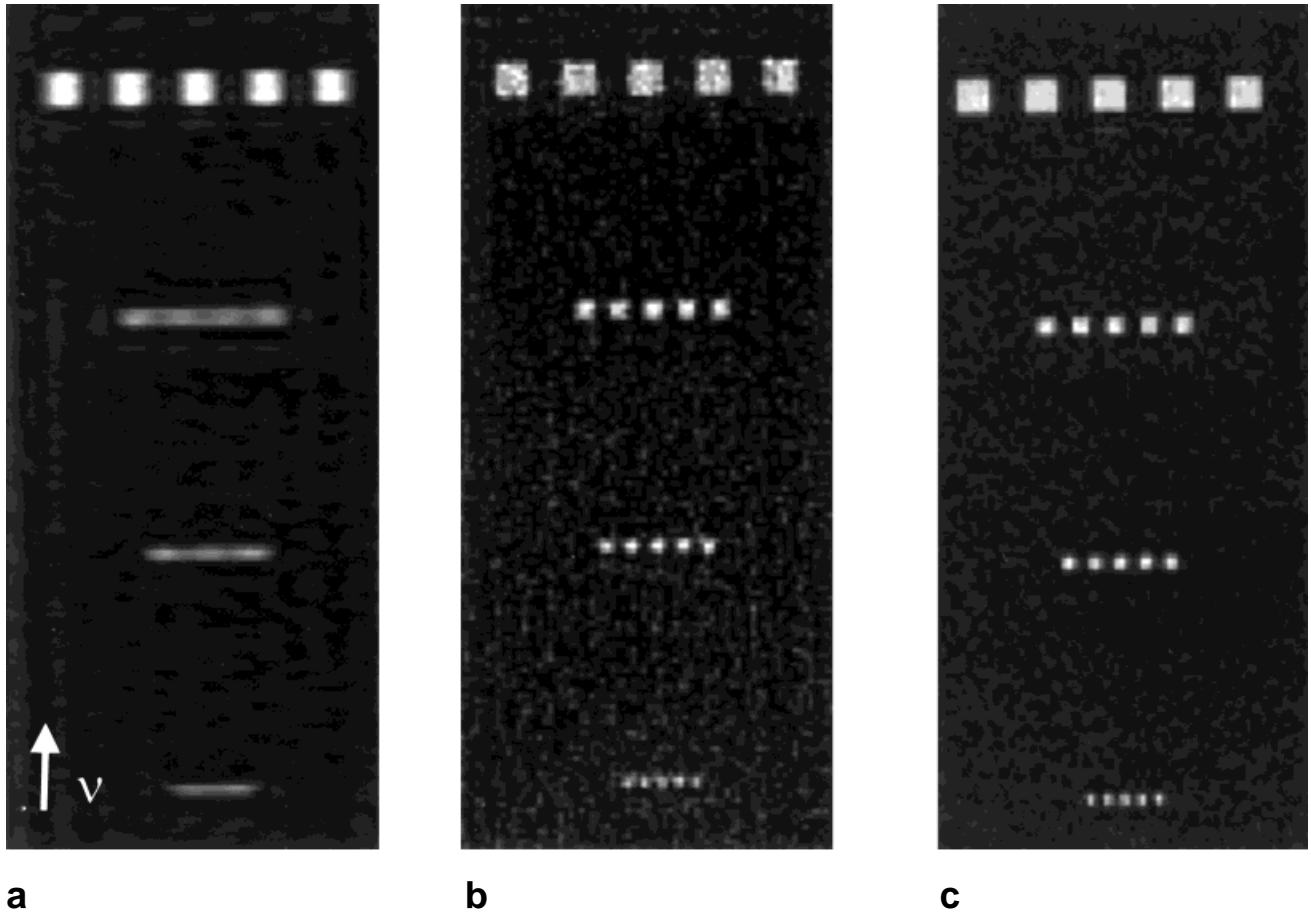
a **b** **c**

FIG. 5. Resolution comparison between FT and PR. **a:** FT 512 × 128 phase encodings. **b:** PR 512 × 128 projections. **c:** FT 512 × 512 phase encodings. The pixel resolution of the 512 × 512 image is 0.3 × 0.3 mm, and the smallest dots are 0.5 mm wide, spaced 0.5 mm apart. The undersampled PR image has resolution similar to the 512 × 512 FT image, although it was acquired in one-fourth of the time. The Fourier frequency-encoding direction is indicated by the arrow.

better resolution than the 400 × 400 FT (512 with 1.3 larger FOV). This places a lower limit on the actual resolution of undersampled PR in this imaging situation.

Human Studies

This section presents the results from four contrast-enhanced exams, out of the 10 exams conducted using PR with contrast agent in healthy volunteers and a patient.

ZIPR With Progressively Fewer Projections

Figure 7 shows the femoral arteries imaged with ZIPR during contrast agent infusion, originally collected as a 512 (312 acquired) × 400 projection angle PR image using the following parameters: 40 × 40 × 11.2 cm FOV, 30° tip, TR/TE of 8.0 ms/1.1 ms, ±64 kHz BW, 312 × 400 projections × 16 k_z × 1 frame acquisition matrix, 512 × 512 × 16 reconstruction matrix, 0.78 × 0.78 × 7.0 mm true voxel size, 51 s scan time, 0.3 mmol/kg at 0.5 ml/s gadolinium contrast agent injection, and torso phased array coil. Images were reconstructed with progressively fewer angles (using (a) 400, (b) 200, (c) 100, and (d) 50 angles) by skipping angles in the full dataset. The changing image quality is due to the worsening of artifacts and reduction of SNR at lower numbers of projections. Nevertheless, clini-
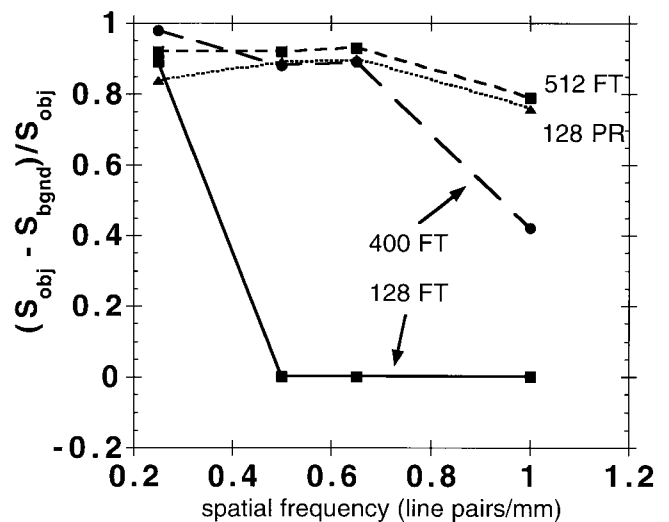
Resolution Comparison for PR and FT

FIG. 6. Quantitative resolution comparison between FT and PR in the resolution phantom for FT acquisitions with 512 phase encodings, 400 phase encodings, 128 phase encodings, and PR with 128 projections. The magnitude of oscillations for each dot pattern is recorded. The 128 PR method performs similarly to the 512 FT method, and better than the 400 FT method.
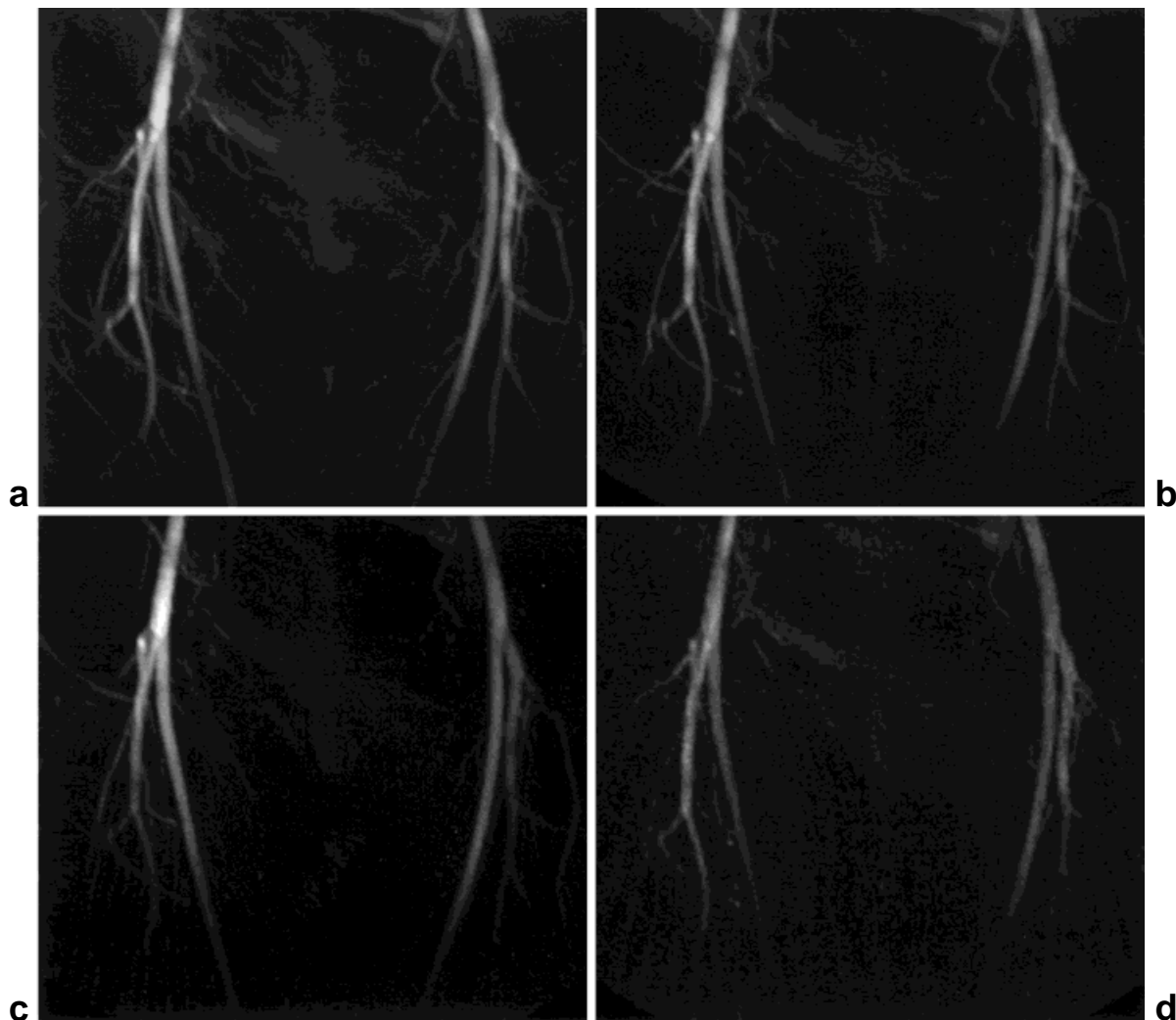
FIG. 7. ZIPR MIPs of the femoral arteries, all generated from the same data set using progressively fewer number of projections: (**a**) 400, (**b**) 200, (**c**) 100, (**d**) 50. Even with 50 projections (**d**), clinically significant detail is present. The origin of the profunda femoral artery at the common femoral artery is well depicted.

cally significant detail is present, even with 50 projections (an undersampling factor of 16 relative to fully sampled PR).

ZIPR Comparisons Between FT and PR in Humans

To evaluate undersampled PR for contrast-enhanced MRA, 3D volumes obtained using the FT and PR imaging methods were compared in a contrast-enhanced scan of the pulmonary vessels. MIP comparisons between FT (512 × 128 phase encodings) and PR (512 × 128 projections) are presented in Fig. 8. The following parameters were used: 36 × 36 × 12.8 cm FOV, 30° tip, TR/TE 7.5 ms/1.2 ms, ±64 kHz BW, 312 × 128 projections or phase encodings × 32 k_z × 1 frame acquisition matrix, 512 × 512 × 64 reconstruction matrix, 0.70 × 0.70 × 4 mm true voxel size for PR, 0.7 × 2.8 × 4 mm true voxel size for FT, 31 s scan time, 18 ml at 1 ml/s gadolinium contrast agent injection, and a torso phased array coil. Minimal undersampling artifact is visible in the PR images. The comparison clearly illustrates significant improvement in resolution for PR in the Fourier phase encoding (horizontal) direction. The FT

MIPs show better SNR and more vessels. The PR images have sharper vessels.

Fast Pulmonary Imaging

One use of undersampled PR is for fast moderate-resolution imaging. For example, patients with suspected pulmonary embolism can only tolerate short breathholds.

In Fig. 9 we compare contrast-enhanced FT and PR pulmonary angiograms both obtained in a 17-sec breathhold. We compare targeted MIPs of the undersampled PR and FT. The scan parameters for PR were: 36 × 36 × 9.6 cm FOV, 40° tip, TR/TE = 6.0 ms/1.2 ms, ±64 kHz BW, 400 (240 acquired) × 170 projections × 16 k_z, 512 × 512 × 32 reconstruction matrix, true voxel size 0.9 × 0.9 × 6 mm, 27 mls at 2 ml/s gadolinium contrast agent injection, fat suppression pulse once per slice loop, and a cardiac phased array coil. For the FT scan (Fig. 9b), all parameters were the same except 256 xres (160 acquired) and a 128 phase encodings resulting in 1.4 × 2.8 × 6.0 mm true voxel size. The comparison shows the much better resolution of
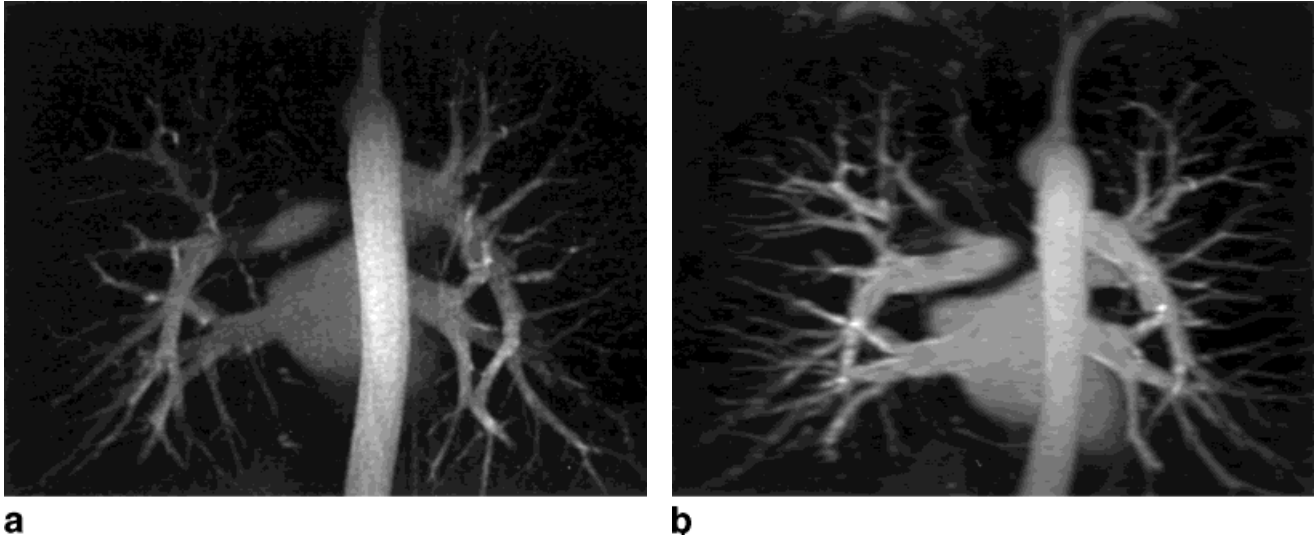
a   **b**

FIG. 8. Comparison of 512 × 128 ZIPR (**a**) and 512 × 128 FT (**b**). The MIPs show the substantial resolution improvement in the Fourier phase encoding (right–left) direction with PR. Both scans used a 0.15 mmol/kg dose of contrast agent and were completed in 30-sec breathholds.

the undersampled PR MIP. The undersampling artifacts are not noticeable in the MIP.

ZIPR Contrast Artifact

Figure 10 shows MIPs from an examination of the femoral arteries that form a temporal series, showing intermediate frame 1.5 (Fig. 10a), frame 2 (Fig. 10b), intermediate frame 2.5 (Fig. 10c) and frame 3 (Fig. 10d). The following parameters were used: 38 × 38 × 6.4 cm FOV, 30° tip, TR/TE of 5.7 ms/1.2 ms, ±64 kHz BW, 312 × 128 projections × 16 k_z × 3 frames acquisition matrix, 512 × 512 × 32 reconstruction matrix, 0.74 × 0.74 × 4 mm true voxel size, 12 s/frame scan time, 15 ml at 2.0 ml/s gadolinium contrast agent injection, and phased array torso coil. The intermediate frames are formed by combining projections from two sequential complete projection sets (see Fig. 4). Frame 2 is the best arterial frame. Frame 3 shows that the contrast agent has begun to wash out. Frame 1.5 shows the early inflow of contrast agent, with only one femoral artery depicted. This is a contrast artifact due to contrast modulation of the projections. The part of the vessel that has dropped out of this early frame is not visible because of its orientation. The projections perpendicular to the vessel, which best represent the vessel, are not yet enhanced in this early frame.

Figure 11 plots a contrast curve generated by the multiframe data (see Eq. [4]) and demonstrates that the contrast agent arrived into the FOV just before frame 2. The optional selection of projections to be grouped and reconstructed in the ZIPR technique should make it possible to reduce the angular dependence shown in frame 1.5. The contrast curve estimate can be used to reweigh the projections in order to provide relatively constant signal for all projections. However, this process can decrease SNR if projections with minimal contrast are included. Two other acquisition methods for avoiding these angularly dependent contrast artifacts are discussed below, interleaved ZIPR and PRIZE.

PRIZE Method

As in Fig. 4, the PRIZE method acquires all of the projections for each partition-encoding. SNR and venous suppression are improved by collecting the low k_z spatial frequencies during peak arterial contrast. Here we present PRIZE in the carotid arteries. Artery–vein separation is particularly difficult in the carotid arteries in a long contrast-enhanced scan since the arterial–venous separation time is only 7 sec. Wilman et al. (22) have shown that it is possible to capture the arterial phase of the carotids using elliptical-centric acquisition and MR fluoroscopic triggering of the acquisition.

Figure 12 shows the PRIZE MIP of carotids, with centric acquisition order in k_z. The full MIP (Fig. 12a) and a reformatted view of the left carotid bifurcation are shown. The following scan parameters were used: 20 × 20 × 5.1 cm FOV, 30° tip, TR/TE 6.3 ms/1.2 ms, ±64 kHz BW, 448 xres (280 acquired) × 128 projections × 32 k_z acquisition matrix, 512 × 512 × 64 reconstruction matrix, 1.6 mm slice thickness, 26 s scan time, 0.3 mmol/kg at 3.0 ml/s gadolinium contrast agent injection, and a head–neck vascular coil. The scan was initiated 15 sec after the start of injection, based on information from a dose-timing scan. The readout resolution was 448 instead of 512 to improve the SNR. The true voxel size was 0.45 × 0.45 × 1.6 mm. This MIP shows little contamination of the jugular veins and indicates that, at least in this 26-sec examination, centric k_z encoding was sufficient to suppress veins.

DISCUSSION

It has been previously recognized in X-ray CT that the use of a decreasing number of projection angles decreases the radius of the alias-free FOV which may be reconstructed but does not decrease spatial resolution (23,24). One CT article states: ''It is now well known that a limited number of views does not directly limit the resolution obtainable.... The effect of a limited number of views is to restrict the
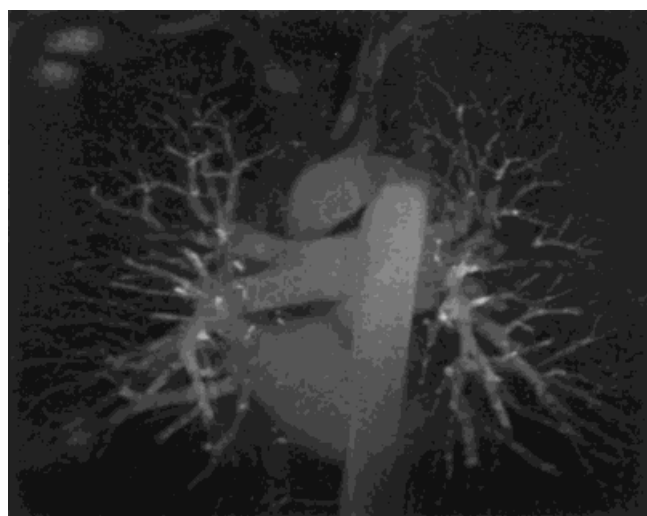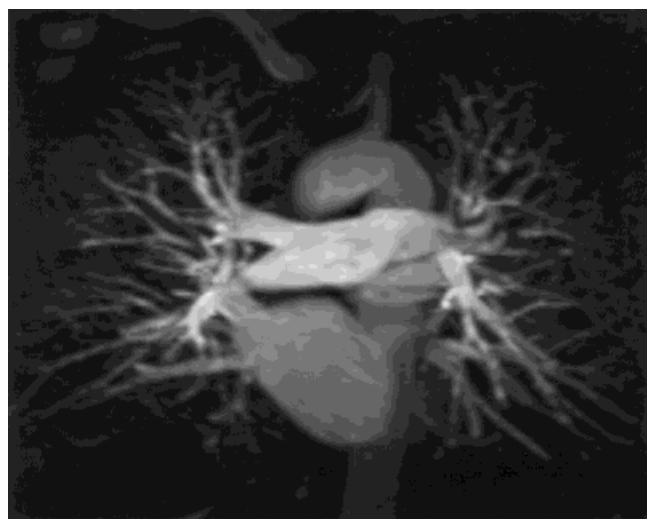
a

b

FIG. 9. Comparison of targeted pulmonary MIPs for 400 × 170 ZIPR (**a**) and 256 × 128 FT (**b**), showing higher resolution using PR in equal scan times. Both scans were completed in a 17-sec breathhold, using a 0.15 mmol/kg dose of contrast agent.

radius of the region over which artifact-free reconstruction is possible....;'' (23, p. 444). The undersampled MRA application presented here is based on the realization that when a large FOV is undersampled, this small FOV behavior occurs throughout the image. Spatial resolution is dependent primarily on readout resolution. This permits rapid acquisition of high-resolution images with the potential disadvantage that individual objects, although they would be correctly reconstructed in a local small FOV, will be contaminated by artifacts from all other objects in the image.

Our initial experience indicates that the combination of undersampled PR and contrast-enhanced MRA might provide a means for acquiring MRAs of higher resolution during the infusion of contrast material, with tolerable artifacts. In phantoms (see Fig. 5), the resolution of undersampled PR (512 × 128) was visually almost equal to that of 512 × 512 FT and significantly better than 512 × 128 FT.

Figure 6 compares the spatial frequency response of 512 × 128 PR to 512 × 512 FT, 400 × 400 FT, and a 512 × 128 FT, showing that undersampled PR has resolution measurably higher than the 400 × 400 FT acquisition. However, the artifacts associated with undersampling reduce the value of greater resolution. In humans, the resolution of PR images is visually higher than FT images for equal scan times, in the Fourier phase encoding direction (Figs. 8, 9).

The artifacts produced by an anatomical configuration of blood vessels depends on the distribution, size, and intensity of these vessels, and on the extent to which the sampling process neglects high spatial frequencies having significant energy. A large object containing predominantly low spatial frequencies will produce less intense artifacts than a small object containing more energy at higher spatial frequencies. In our work in contrast-enhanced MRA, typically using a minimum of 100 projection angles, the artifacts appear to be tolerable, even though in X-ray CT the artifacts associated with undersampled PR were large compared to the attenuation differences to be distinguished. The artifacts must be examined in each contemplated clinical application. The processes of mask subtraction, background suppression, fat saturation, and
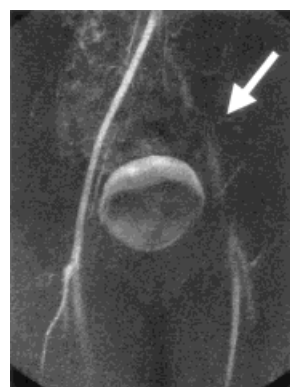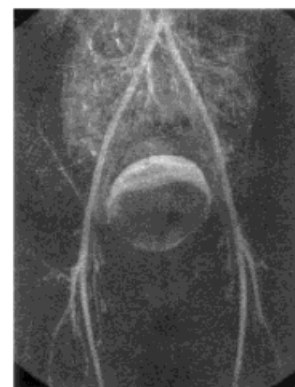

a frame 1.5

b frame 2

c frame 2.5

d frame 3

FIG. 10. A temporal series of MIPs obtained with the ZIPR sequence. Frames 1.5 (**a**) and 2.5 (**c**) were reconstructed using shared projections from sequential acquired sets. In frame 1.5 the first half of the projections were acquired prior to the arrival of adequate contrast agent, leading to loss of signal in one of the iliac arteries (arrow). Frame 2 (**b**) is the best arterial frame. In frames 2.5 (**c**) and 3 (**d**) the contrast agent is beginning to wash out.
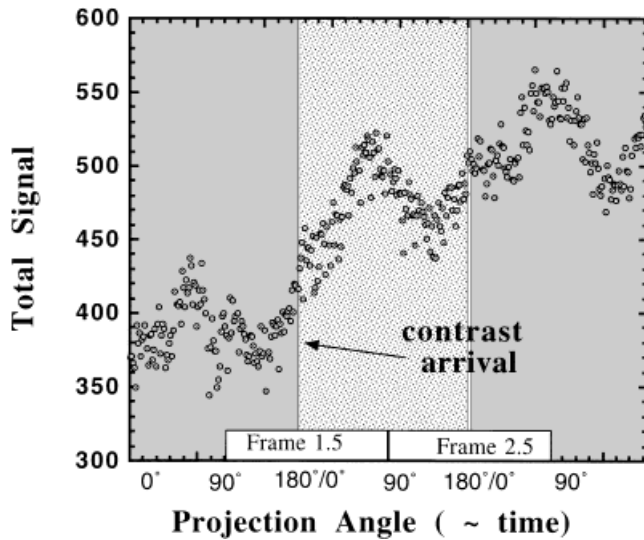
FIG. 11. The contrast curve for the multiphase femoral artery study showing the time periods for each reconstructed frame. Each frame consisted of 128 projections, acquired in 12 sec. The contrast agent arrives shortly before the start of frame 2.

est signals in the image and are predictable based on knowledge of the data acquisition and reconstruction processes. If an estimate image of these bright objects can be found, for example by application of a threshold on the image, an image of these objects and their associated undersampling artifacts can be generated by reprojecting the objects with the same limited number of angles and performing filtered backprojection. The artifacts can be isolated and then subtracted from the original image. In X-ray CT, this type of artifact-reduction method was proposed for cardiac imaging (25), using a fully sampled reference image.

We have previously demonstrated that the proposed undersampled projection reconstruction also leads to a resolution increase in noncontrast-enhanced MRA (15). For example, in 3D acquisitions of equal duration, undersampled PR MRA can potentially produce in-plane resolution equal to that of FT imaging but provide four times the resolution in the slice direction. This could have important implications for intracranial imaging provided that the artifacts are acceptable.

The gains in spatial resolution provided by PR are offset by reduced overall SNR. This is due to the linear dependence of SNR on voxel size and the use of high bandwidth acquisitions to reduce off-resonance blurring. Furthermore, the streak artifacts generated by the structures in each slice may contribute to a diffuse, unwanted signal that acts like noise to degrade image quality. The SNR reduction at high resolution and the diffuse unstructured streak artifacts appear to be more serious than the structured streak artifacts from bright objects.

MIP reduce the amount of artifacts. Enhanced vasculature from outside the FOV, but within the region of receiver sensitivity, adds artifact.

An algorithm for the reduction of artifacts might permit more aggressive undersampling, leading to further increases in the rate at which high-resolution images can be acquired. The artifacts emanate primarily from the bright-
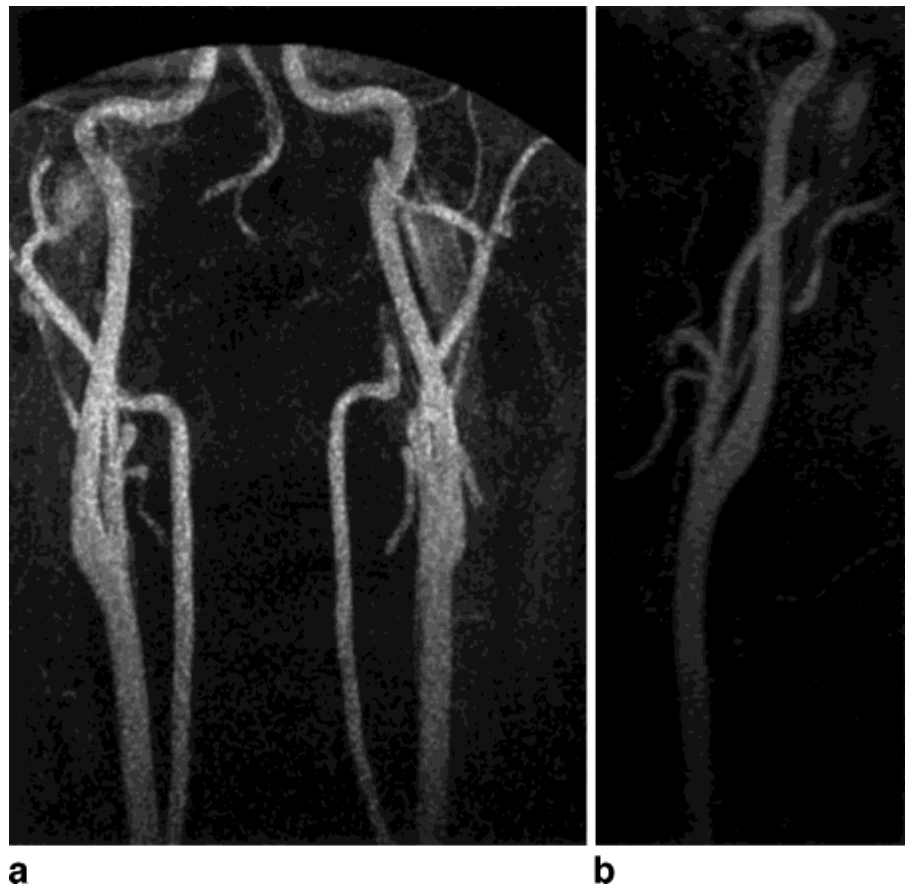
FIG. 12. A PRIZE study of the carotid arteries using k_z-centric acquisition. The jugular veins are not apparent even though the acquisition took 26 sec. **a:** The MIP. **b:** A reformatted view of the carotid bifurcation. Voxel size is 0.45 × 0.45 × 1.6 mm.

a

b

This adverse decrease in SNR with increased resolution is only true for large objects. For objects smaller than the voxel defined by the acquisition matrix, SNR no longer decreases in inverse proportion to voxel size. Consider an object with dimensions of one pixel in a 512×512 array. This object will have double the SNR in a 512×512 FT acquisition as in a 512×128 FT acquisition. For objects much larger than a pixel, we would expect the 512 acquisition to have half the SNR of the 128 acquisition due to the combined effects of pixel size and acquisition time. For the case of the small object, losses in SNR from increasing resolution are alleviated by the improved system modulation transfer function that adequately records the spatial frequencies of the object. The same effect causes a 128 angle PR sequence producing a 512×512 reconstruction matrix and a 512×128 FT acquisition to image this small object with a similar SNR. PR has slightly lower SNR than FT for identical scan parameters (including voxel size) due to the nonuniform sampling of k-space (18).

For contrast-enhanced MRA, the ability to rapidly acquire high-resolution images might be advantageously combined with rapid injection of contrast agent. For contrast-enhanced MRA, so long as TR $<<$ T_1, scan time reduction is possible without SNR reduction, because SNR is related to contrast dose (26,27): for shorter scan times, higher injection rates are possible. Higher injection rates increase SNR provided that additional T_2^* losses are not large. The technique reported here promises to become more and more feasible as advances in surface coil design or other means to increase SNR are realized.

We have presented two strategies for the acquisition of PR data during contrast agent infusion. The placement of central k_z data at peak arterial contrast in the PRIZE method appears to be adequate for removal of venous signal in the carotid artery examinations, as indicated in Fig. 12, even though an acquisition time of 26 sec was used. Because of the small rectangular FOV used for imaging the carotids, relatively high resolution is readily obtainable using current FT methods. Increased resolution, as obtained in the PRIZE carotids of Fig. 12, may be currently unsupportable in terms of SNR. The temporal resolution needed for artery–vein separation in the carotids is achievable using other methods (22,28). More temporal resolution may be added to the PRIZE acquisition by incorporating a k_z sampling scheme and temporal interpolation, as used in our previously reported 3D TRICKS method (28). This application (29) (PR TRICKS) could potentially provide temporal resolution while at the same time providing higher spatial resolution than conventional FT techniques. The role of SNR will be an important consideration in this application and might limit the temporal or spatial resolution that can be supported by the acquired data.

The multiframe ZIPR method in conjunction with contrast agents involves a k-space weighting different from that of FT or PRIZE. The ZIPR property of acquiring high and low spatial frequencies throughout the scan means that if projections are acquired following venous enhancement and used in the reconstruction, some central k-space with venous weighting will be obtained at those angles. This will not happen in a properly timed FT or PRIZE acquisition.

Unlike PRIZE, where all projections for a given partition encoding are acquired in a brief period of time, typically 1 sec or less, ZIPR images can suffer from a new angle-dependent contrast artifact because of the use of unenhanced projections. When this occurs, one must either normalize the various projections based on the contrast curve estimate or choose later projection sets that have more uniform contrast. This will be possible if the injection time is matched to the acquisition time. The latter is preferable if venous contamination does not interfere, since reweighting of projections with inadequate contrast decreases SNR.

A potential remedy for ZIPR contrast modulation and venous contamination is to acquire multiple interleaved projection sets, each representing a complete angular range, but having a small angular offset. This acquisition method was proposed by Rasche et al. (3) for motion imaging. To reduce venous contamination, each of these sets can be reconstructed to provide an image with a smaller temporal window but greater artifacts. Those projection sets acquired before venous contamination can be combined to form a set containing a greater number of projections. Using only adequately enhanced interleaved projection sets might reduce the problem of angularly dependent contrast weighting. This would result in more uniform angular weighting of k-space. We are currently investigating this acquisition method (30).

Acquisitions with smooth contrast-modulation of k-space and greatest enhancement of central k-space provide the best contrast-enhanced images (22,31). The PRIZE method has advantages over the multiframe ZIPR method, inasmuch as it allows centric acquisition to reduce venous signal, and has no angle-dependent artifacts. With ZIPR, centric acquisitions are not possible, and k-space is modulated angularly. However, the acquisition of more than one complete set of angles or the use of interleaved angular sets provides flexibility with regard to the position of the reconstructed projections relative to the contrast curve.

CONCLUSIONS

We have presented an alternative MRA method using undersampled projection reconstruction. It has the advantage of obtaining greater resolution per unit time relative to FT. The observed artifact level in contrast-enhanced MRA images appears to be acceptable in the applications we have investigated. PRIZE provides the opportunity for a timed or triggered high-resolution scan acquired in a manner similar to 3D FT MRA but with potentially higher spatial resolution and adequate venous rejection. ZIPR provides temporally resolved high-resolution images and the option for retrospective reconstruction of projection sets optimally placed relative to the contrast curve. Undersampled PR provides resolution that is relatively independent of imaging time, at the expense of artifacts.

REFERENCES

1. Lauterbur P, Lai C-M. Zeugmatography by reconstruction from projections. IEEE Trans Nucl Sci 1980;NS-27:1227–1231.
2. Glover GH, Pauly JM. Projection reconstruction techniques for reduction of motion effects in MRI. Magn Reson Med 1992;28:275–289.
3. Rasche V, de Boer RW, Holz D, Proksa R. Continuous radial data acquisition for dynamic MRI. Magn Reson Med 1995;34:754–761.
4. Shimizu K, Mulkern RW, Oshio K, Panych LR, Yoo SS, Kikinis R, Jolesz FA. Rapid tip tracking with MRI by a limited projection reconstruction technique. J Magn Reson Imaging 1998;8:262–264.
5. Rasche V, Holz D, Kohler J, Proksa R, Roschmann P. Catheter tracking using continuous radial MRI. Magn Reson Med 1997;37:963–968.
6. Bergin CJ, Noll DC, Pauly JM, Glover GH, Macovski A. MR imaging of lung parenchyma: a solution to susceptibility. Radiology 1992;183:673–676.
7. Shattuck MD, Gewalt SL, Glover GH, Hedlund LW, Johnson GA. MR microimaging of the lung using volume projection encoding. Magn Reson Med 1997;38:938–942.
8. Gewalt SL, Glover GH, Hedlund LW, Cofer GP, MacFall JR, Johnson GA. MR microscopy of rat lung using projection reconstruction. Magn Reson Med 1993;29:99–106.
9. Edelstein WA, Hutchinson JM, Johnson G, Redpath T. Spin warp NMR imaging and applications to human whole-body imaging. Phys Med Biol 1980;25:751–756.
10. Lai C-M. Reconstructing NMR images from projections under inhomogeneous magnetic fields and non-linear gradients. Phys Med Biol 1983;28:925–938.
11. Hu X, Parrish T. Reduction of FOV for dynamic imaging. Magn Reson Med 1994;31:691–694.
12. Fredrickson JO, Pelc NJ. Temporal resolution improvement in dynamic imaging. Magn Reson Med 1995;35:621–625.
13. Scheffler K, Hennig J. Reduced circular field-of-view imaging. Magn Reson Med 1998;40:474–480.
14. Weiß S, Rasche V. Projection reconstruction reduces FOV imaging. Magn Reson Imaging 1999;17:517–525.
15. Peters DC, Mistretta CA, Korosec FR, Holden J, Kelcz F, Wedding KL, Grist TM, Using projection reconstruction with a limited number of projections to increase image resolution or acquisition speed. In: Proceedings of the ISMRM Sixth Scientific Meeting, Sydney, 1998. p 182.
16. Maki JH, Prince MR, Londy FJ, Chenevert TL. The effects of time varying intravascular signal intensity and k-space acquisition order on three-dimensional MR angiography image quality. J Magn Reson Imaging 1996;6:642–651.
17. Joseph PM. Sampling errors in projection reconstruction MRI. Magn Reson Med 1998;40:460–466.
18. Lauzon ML, Rutt BK. Polar sampling in k-space: reconstruction effects. Magn Reson Med 1998;40:769–782.
19. Noll DC, Nishimura DG, Macovski A. Homodyne detection in magnetic resonance imaging. IEEE Trans Med Imaging 1991;10:154–163.
20. Block WF, Peters DC, Vigen KK. Homodyne reconstruction for projection reconstruction trajectories. In: Proceedings of the ISMRM Seventh Scientific Meeting, Philadelphia, 1999. p 659.
21. Hurst GC, Hua J, Simonetti OP, Duerk JL. Signal-to-noise, resolution and bias function analysis of asymmetric sampling with zero-padded magnitude FT reconstruction. Magn Reson Med 1992;27:247–269.
22. Wilman AH, Riederer SJ, Huston J, Wald JT, Debbins JP. Arterial phase carotid and vertebral artery imaging in 3D contrast-enhanced MR angiography by combining fluoroscopic triggering with an elliptical centric acquisition order. Magn Reson Med 1998;40:24–35.
23. Joseph PM, Whitley J. Experimental simulation of ECG-gated heart scans with a small number of views. Med Phys 1983;10:444–449.
24. Smith P, Peters T, Bates R. Image reconstruction from finite number of projections. J Phys A Nucl Gen 1973;6:361–375.
25. Garden KL, Robb RA. 3-D Reconstruction of the heart from few projections: a practical implementation of the McKinnon-Bates algorithm. IEEE Trans Med Imaging 1986;5:233–239.
26. Parker DL, Goodrich KC, Alexander AL, Buswell HR, Blatter DD, Tsuruda JS. Optimized visualization of vessels in contrast enhanced intracranial MR angiography. Magn Reson Med 1998;40:873–882.
27. Pelc NJ, Alley MT, Shifrin RY, Herfkens RJ. Outer limits of contrast-enhanced MRA, revisited. In: Proceedings of the ISMRM 6th Scientific Meeting, Sydney, 1998. p 98.
28. Korosec FR, Frayne R, Grist TM, Mistretta CA. Time-resolved contrast-enhanced 3D MR angiography. Magn Reson Med 1996;36:345–351.
29. Vigen KK, Peters DC, Grist TM, Block WF, Mistretta CA. Undersampled projection imaging for time-resolved contrast-enhanced 3D MR angiography (PR-TRICKS). In: Proceedings of the ISMRM Seventh Scientific Meeting, Philadelphia, 1999. p 1899.
30. Peters DC, Grist TM, Korosec FR, Holden J, Block WF, Wedding KL, Carroll TJ, Mistretta CA. Undersampled projection reconstruction applied to MR angiography. In: Proceedings of the ISMRM 7th Scientific Meeting, Philadelphia, 1999. p 153.
31. Mistretta CA, Grist TM, Korosec FR, Frayne R, Peters DC, Mazaheri Y, Carroll TJ. 3D Time-resolved contrast-enhanced MR DSA: advantages and tradeoffs. Magn Reson Med 1998;40:571–581.